Journal of Organometallic Chemistry 695 (2010) 2126–2133

Contents lists available at ScienceDirect

Journal of Organometallic Chemistry

journal homepage: www.elsevier.com/locate/jorganchem

A density functional theory study of the oxidative addition of methyl iodide to square planar [Rh(acac)(P(OPh)$_3$)$_2$] complex and simplified model systems

Marrigje M. Conradie [a], Jeanet Conradie [a,b,*]

[a] Department of Chemistry, University of the Free State, 9300 Bloemfontein, Republic of South Africa
[b] Department of Chemistry and Centre for Theoretical and Computational Chemistry, University of Tromsø, N-9037 Tromsø, Norway

ARTICLE INFO

Article history:
Received 18 January 2010
Received in revised form
14 May 2010
Accepted 20 May 2010
Available online 27 May 2010

Keywords:
Density functional
Rhodium
Oxidative addition
Phosphite
Acetylacetone

ABSTRACT

The transition state for the oxidative addition reaction [Rh(acac)(P(OPh)$_3$)$_2$] + CH_3I, as well as two simplified models *viz.* [Rh(acac)(P(OCH$_3$)$_3$)$_2$] and [Rh(acac)(P(OH)$_3$)$_2$], are calculated with the density functional theory (DFT) at the PW91/TZP level of theory. The full experimental model, as well as the simplified model systems, gives a good account of the experimental Rh-ligand bond lengths of both the rhodium(I) and rhodium(III) β-diketonatobis(triphenylphosphite) complexes. The relative stability of the four possible rhodium(III) reaction products is the same for all the models, with *trans*-[Rh(acac)(P(OPh)$_3$)$_2$(CH$_3$)(I)] (in agreement with experimental data) as the most stable reaction product. The best agreement between the theoretical and experimental activation parameters was obtained for the full experimental system.

1. Introduction

The oxidative addition reaction of covalent molecules (such as alkyl halides) to low-valent transition metal complexes, is a fundamental process in homogenous catalysis. A well-known example is the oxidative addition of methyl iodide to *cis*-[Rh(CO)$_2$I$_2$]$^-$ [1]. This methanol carbonylation process with the original Monsanto catalyst has been studied in detail both experimentally [2,3] and theoretically [3–7]. In contrast, the same reaction promoted from β-diketonatobis(triphenylphosphite)rhodium(I) complexes, has only been the subject of detailed experimental research [8].

It is widely accepted that oxidative addition of methyl iodide to square planar rhodium(I) complexes occurs *via* a two-step mechanism (Fig. 1) involving (i) nucleophilic attack by the metal on the methyl carbon to displace iodide to form a metal-carbon bond, presumed to proceed with inversion of configuration at the carbon and (ii) coordination of iodide to the five-coordinated intermediate to give a six-coordinated alkyl complex [3,7,9]. This mechanism results in the *trans* addition of the methyl iodide to the square planar rhodium(I) complex. The observation of *cis* products has sometimes been taken as evidence for an alternative concerted three-center mechanism leading to retention of configuration at the carbon [10].

Experimentally determined large negative values of the volume ($\Delta V^{\neq}$) and the entropy ($\Delta S^{\neq}$) of activation for the oxidative addition reaction of CH_3I to a series of [Rh(β-diketonato)(P(OPh)$_3$)$_2$] complexes, indicated a mechanism which occurs *via* a polar transition state [8b] which is consistent with the S_N2 mechanism [11]. On grounds of ^{1}H NMR data, the structure of the product of the oxidative addition, [Rh(β-diketonato)(P(OPh)$_3$)$_2$(CH$_3$)(I)], is proposed to adopt an octahedral geometry in which the β-diketonato ligand and the two triphenylphosphite groups are located in an equatorial plane with the methyl and iodide ligands in the axial positions [8]. No solid state X-ray crystal structure has been solved for the product [12]. Since the understanding of the mechanism of activity of a catalyst requires an understanding of its structure in all reaction steps, we have undertaken a density functional theory study of the geometry of the reactant, transition state and possible products of the oxidative addition reaction of CH_3I to [Rh(acac)(P(OPh)$_3$)$_2$] (where Hacac = acetylacetone). Due to the computational demand of optimizing such a big molecular system, we were specifically interested in determining whether simplified models of [Rh(acac)(P(OPh)$_3$)$_2$] give the same information regarding the nature of the transition state and possible reaction products of the oxidative addition reaction in this study.

* Corresponding author at: Department of Chemistry, University of the Free State, 9300 Bloemfontein, Republic of South Africa. Tel.: +27 51 4012194; fax:+27 4446384.
E-mail address: conradj@ufs.ac.za (J. Conradie).

0022-328X/$ – see front matter © 2010 Elsevier B.V. All rights reserved.
doi:10.1016/j.jorganchem.2010.05.021

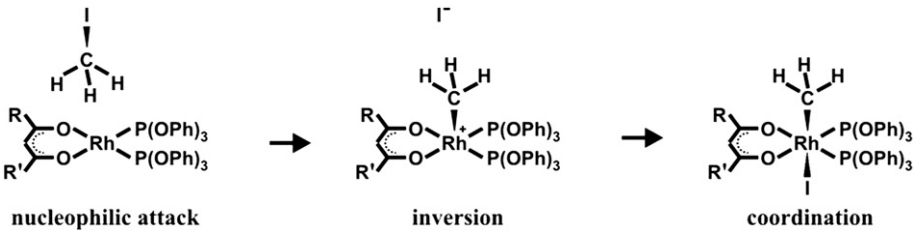

Fig. 1. S_N2 Mechanism for the oxidative addition of methyl iodide to a square planar β-diketonatobis(triphenylphosphite)rhodium(I) complex.

2. Computational details

DFT calculations were carried out using the ADF (Amsterdam Density Functional) 2007 programme [13] with the GGA (Generalised Gradient Approximation) functional PW91 (Perdew-Wang, 1991) [14]. The TZP (Triple ζ polarised) basis set, with a fine mesh for numerical integration, a spin-restricted formalism and full geometry optimization with tight convergence criteria, was used for minimum energy and transition state (TS) searches. Approximate structures of the TS have been determined with linear transit (LT) scans, with a constrained optimization along a chosen reaction coordinate, to sketch an approximate path over the TS between reactants and products. Throughout, all calculations have been performed with no symmetry constraint (C_1) and all structures have been calculated as singlet states.

Numerical frequency analyses [15,16], where the frequencies are computed numerically by differentiation of energy gradients in slightly displaced geometries, have been performed to verify the TS geometries. A TS has one imaginary frequency.

Zero point energy and thermal corrections (vibrational, rotational and translational) were made in the calculation of the thermodynamic parameters. The enthalpy (H) and Gibbs free energy (G) were calculated from

$$U = E_{TBE} + E_{ZPE} + E_{IE} \quad (1)$$

$$H = U + RT \text{ (gas phase) or } H = U \text{ (solution)} \quad (2)$$

$$G = H - TS \quad (3)$$

where U is the total energy, E_{TBE} is total bonding energy, E_{ZPE} is zero point energy, E_{IE} is internal energy (sum of vibrational, rotational and translational energies), R is the gas constant, T is temperature and S is entropy. The entropy (S) was calculated from the temperature dependent partition function in ADF at 298.15 K. The computed results assume an ideal gas.

Solvent effects were taken into account for all calculations reported here. The COSMO (Conductor like Screening Model) model of solvation [17–19] was used as implemented in ADF [20]. The COSMO model is a dielectric model in which the solute molecule is embedded in a molecule-shaped cavity surrounded by a dielectric medium with a given dielectric constant (ε_0). The type of cavity used is Esurf [21] and the solvent used is methanol ($\varepsilon_0 = 32.6$). Where applicable, scalar relativistic effects were used with the ZORA [22–26], (Zero Order Regular Approximation) formalism.

The accuracy of the computational approach was evaluated by comparing the root-mean-square distances (RMSDs) as calculated by the "RMS Compare Structures" utility in ChemCraft [27]. The RMSD values were calculated for the best three-dimensional superposition of optimized molecular structures on experimental crystal structures, using only the non-hydrogen atoms and the non-rotational groups of the molecule.

3. Results and discussion

3.1. Study of β-diketonatobis(triphenylphosphite)rhodium complexes

Since density functional computational methods to the knowledge of the author are for the first time applied to [Rh(β-diketonato)(P(OPh)$_3$)$_2$] complexes and reported here, some measure of the reliability of the approach had to be obtained. This was addressed by comparing the known single crystal X-ray diffraction structure (Fig. 2) of [Rh^{I}(β-diketonato)(P(OPh)$_3$)$_2$] (β-diketonato = acac [28] (**1**), tfba [29] (**2**), tfaa [30] (**3**)) and [Rh^{III}(β-diketonato)(P(OPh)$_3$)$_2$(I)$_2$] (β-diketonato = tfaa [31] (**4**)) (Htfba = trifluorobenzoylacetone and Htfaa = trifluoroacetylacetone) with the theoretically calculated structure of the same complex.

Complexes **1**, **3** and **4** crystallized with two molecules in the asymmetric unit. When comparing the backbones of the two molecules in the asymmetric unit (*i.e.*, [Rh(CCOCCOC)(P)$_2$]) a RMSD value of 0.03, 0.06 and 0.13 Å is obtained respectively for **1**, **3** and **4**. Inclusion of the O atoms on the P (*i.e.,* [Rh(CCOCCOC)(PO$_3$)$_2$]) gives a RMSD value of 0.04, 0.61 and 0.19 Å respectively. Note that the backbones of the two molecules in the asymmetric unit are near enantiomers and therefore the mirror symmetry of the one crystal of each was used for the fitting. The larger RMSD values, when the O atoms on the P are included, indicate that packing in the solid state may give rise to different orientations of the OPh groups, whereas in solution these OPh groups can rotate freely. Care should therefore be taken when optimizing these types of molecules when the geometry is not experimentally known (no experimental crystal structure), that the global minimum energy geometry is obtained and not a local minimum structure, due to the orientation of the OPh groups. The relative energy of the two enantiomeric molecules in the asymmetric unit, optimized with and without relativistic effects in methanol as solvent, is virtually the same, as would be expected for near enantiomers (Table 1).

The theoretical and experimental geometrical data of complexes **1**–**4** are summarized in Table S1 and comparative information with signed deviations is given in Table S2 (atom numbering is as indicated

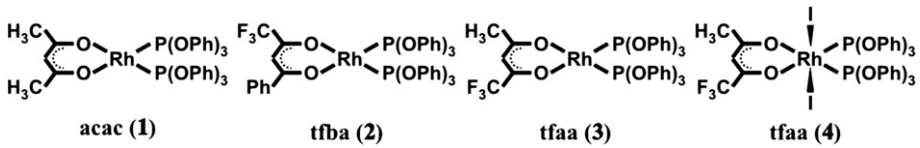

Fig. 2. Schematic illustration of β-diketonatobis(triphenylphosphite)rhodium complexes that have been solved by X-ray crystallography [28–31].

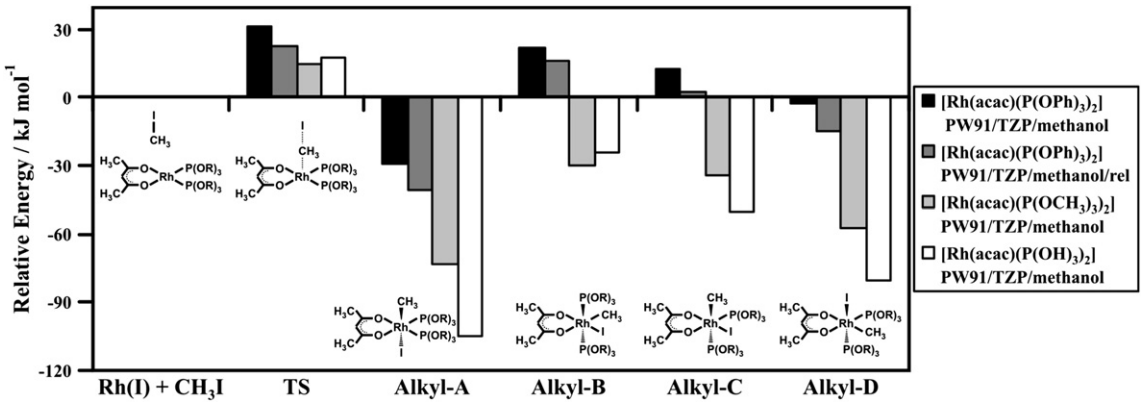

Fig. 3. The PW91/TZP/methanol calculated energies (ΔE_{TBE}) of the reactants [Rh(acac)(P(OR)$_3$)$_2$] + CH$_3$I, the TS and the four possible [Rh(acac)(P(OR)$_3$)$_2$(CH$_3$)(I)]-alkyl reaction products. The energy of the reactants is taken as zero. Values are listed in Table 2.

in Fig. S1, see Supporting information). High agreement between experimental and theoretical structures is obtained, as reflected by the RMSD values of the calculated data superimposed on the experimental data of less than 0.11 Å. A key indicator in organometallic compounds is the bond lengths and angles involving the metal center. The bonds in the coordination polyhedron of **1**–**4** were generally slightly overestimated by the DFT calculations (0.00–0.10 Å for Rh–O bonds and 0.02–0.10 Å for Rh–P bonds). It is well-known that GGA density functionals overestimate bonds lengths [32]. The angles around the Rh were calculated accurately within 2.9°. The calculations including relativistic effects gave more precise bond lengths than the calculation without relativistic effects (Table S2). Here it is informative to notice that the Rh–O and Rh–P bonds (or angles around the Rh) of the optimized geometries of the two enantiomeric molecules in the asymmetric unit *i.e.*, **1**, **3** or **4** differ by 0.00–0.01 Å and 0°–3°. Since comparisons of experimental metal–ligand bond lengths with calculated bond lengths below a threshold of 0.02 Å are considered as meaningless [33], the methods employed in this study therefore give a good account of the experimental bond lengths of both rhodium(I) and rhodium(III) β-diketonatobis(triphenylphosphite) complexes.

Oxidative addition of CH$_3$I to [Rh(acac)(P(OPh)$_3$)$_2$] (**1**) leads to an alkyl product [Rh(acac)(P(OPh)$_3$)$_2$(CH$_3$)(I)]. Four possible rhodium(III) alkyl isomers are possible: one (Alkyl-A) if *trans* addition occurs and three possible isomers (Alkyl-B, Alkyl-C and Alkyl-D) if *cis* addition occurs (inserts in Fig. 3) [34]. Due to the computational demand for optimizing such a big molecular system, we introduced two simplified models of [Rh(acac)(P(OPh)$_3$)$_2$] (**1**), *viz.* [Rh(acac)(P(OCH$_3$)$_3$)$_2$] and [Rh(acac)(P(OH)$_3$)$_2$]. The goal is to determine whether the simplified models give the same information regarding the nature, geometry and energetics of the TS and products of oxidative addition.

3.2. Energy profile of the acetylacetonatobis(triphenylphosphite) rhodium and simplified models

The PW91/TZP/methanol optimized relative energies of the rhodium(I) complex [Rh(acac)(P(OPh)$_3$)$_2$] (**1**) and the four possible rhodium(III) isomers [Rh(acac)(P(OPh)$_3$)$_2$(CH$_3$)(I)] of the full experimental model (R = Ph) are displayed in Fig. 3 with the values tabulated in Table 2. These results indicate (in agreement with experimental observation) [8] that the *trans* product Alkyl-A is the product of oxidative addition of CH$_3$I to [Rh(acac)(P(OPh)$_3$)$_2$]. The two simplified systems [Rh(acac)(P(OCH$_3$)$_3$)$_2$] and [Rh(acac)(P(OH)$_3$)$_2$] (also displayed in Fig. 3) show the same trend regarding the relative energies of the four possible rhodium(III) reaction products, *viz.* (most stable) Alkyl-A < Alkyl-D < Alkyl-C < Alkyl-B. Inclusion of relativistic effects in the calculations did not change the relative stability of the four possible [Rh(acac)(P(OR)$_3$)$_2$(CH$_3$)(I)] products for all three models (R = Ph, CH$_3$ or H). The energetically preferred product of the oxidative addition reaction of CH$_3$I to [Rh(acac)(P(OPh)$_3$)$_2$] therefore assumes an octahedral geometry, with the β-diketonato and the two triphenylphosphite groups located in the equatorial plane and the methyl and iodide ligands in the axial position. The *trans* addition of CH$_3$I to [Rh(β-diketonato)(P(OPh)$_3$)$_2$] is also confirmed by the structure determination of a similar complex, *trans*-[Rh(*N*-benzoyl-*N*-phenylhydroxyamino)(P(OPh)$_3$)$_2$(CH$_3$)(I)] [35]. Oxidative addition of I$_2$ to [Rh(tfaa)(P(OPh)$_3$)$_2$] also gave the *trans* product (Fig. 2 complex 4) [31]. DFT calculations on the structurally similar rhodium-β-diketonato complexes, [Rh(β-diketonato)(CO)(PPh$_3$)] with β-diketone = 4,4,4-trifluoro-1-(2-thenoyl)-1,3-propanedione, 1-phenyl-3-(2-thenoyl)-1,3-propanedione, 1,3-di(2-thenoyl)-1,3-propanedione and 1-ferrocenyl-4,4,4-trifluorobutane-1,3-dione, in agreement with experimental observations, also found *trans* addition of CH$_3$I to the square planar rhodium(I) complexes [36].

3.3. Geometry of acetylacetonatobis(triphenylphosphite)rhodium and simplified models

The PW91/TZP/methanol optimized geometrical data for the full experimental model (R = Ph) are illustrated in Fig. 5 and the bond lengths and bond angles around the Rh center of all three models (R = Ph, CH$_3$ or H) are given in Table 2. Introducing R = CH$_3$ or H instead of Ph, did not change the bond lengths around the Rh center significantly – the calculated bond lengths were similar within 0.05 Å. The bond angles around the Rh center were within 8.5° (5%)

Table 1
The relative energies (kJ mol^{-1}) of the DFT optimized structures of the two enantiomeric molecules in the asymmetric unit of **1**, **3** and **4**.

	[Rh(acac)(P(OPh)$_3$)$_2$ (**1**)		[Rh(tfaa)(P(OPh)$_3$)$_2$ (**3**)		[Rh(tfaa)(P(OPh)$_3$)$_2$(I)$_2$ (**4**)	
	Molecule 1	Molecule 2	Molecule 1	Molecule 2	Molecule 1	Molecule 2
PW91/TZP/methanol[a]	0.0	1.7	0.0	3.8	0.6	0.0
PW91/TZP/methanol/rel[b]	0.0	2.5	0.0	1.7	2.4	0.0

[a] Geometry optimization was done with the PW91 functional and the TZP basis set in methanol as solvent.
[b] Geometry optimization under the same conditions as (***a***), but with inclusion of relativistic effects.

Table 2
A comparison between the PW91/TZP/methanol calculated minimum energy geometries of the [Rh(acac)(P(OR)$_3$)$_2$] complex and the four possible [Rh(acac)(P(OR)$_3$)$_2$(CH$_3$)(I)]-alkyl reaction products for R = Ph, CH$_3$ and H. Angles (°), bond lengths (Å) and RMSD values (Å) are as indicated. All models were optimized without relativistic effects, except where indicated. The RMSD value was calculated by fitting the Rh(CCOCCOC)(P)$_2$ backbones of the simplified models on the backbone of the full model (R = Ph). The calculated energies (ΔE_{TBE} in kJ mol^{-1}) are also listed with the energy of the reactant taken as zero (see Fig. 3).

		Ph	Ph (incl. rel.)	CH_3	H
Rh(I)	Rh–P	2.195	2.171	2.218	2.189
	Rh–P′	2.194	2.171	2.217	2.196
	Rh–O	2.097	2.071	2.113	2.119
	Rh–O′	2.096	2.071	2.111	2.117
	O–Rh–O′	89.9	90.0	89.1	90.6
	O′–Rh–P′	88.8	88.4	91.0	87.4
	P′–Rh–P	92.6	93.1	92.6	93.6
	P–Rh–O	88.7	88.5	87.3	87.9
	RMSD	–	0.02	0.06	0.09
	ΔE_{TBE}	0	0	0	0
Alkyl-A	Rh–P	2.277	2.250	2.270	2.239
	Rh–P′	2.271	2.240	2.270	2.244
	Rh–O	2.117	2.099	2.127	2.143
	Rh–O′	2.105	2.086	2.126	2.136
	Rh–I	2.889	2.855	2.943	2.913
	Rh–C	2.121	2.110	2.104	2.114
	O–Rh–O′	91.2	91.4	90.1	90.6
	O′–Rh–P′	88.3	88.3	88.5	85.6
	P′–Rh–P	96.5	96.6	93.2	97.8
	P–Rh–O	83.8	83.6	87.9	86.0
	I–Rh–C	169.1	168.4	171.7	176.5
	RMSD	–	0.02	0.12	0.15
	ΔE_{TBE}	−28	−40	−71	−101
Alkyal-B	Rh–P	2.348	2.317	2.344	2.312
	Rh–P′	2.351	2.321	2.354	2.335
	Rh–O	2.187	2.165	2.203	2.190
	Rh–O′	2.092	2.075	2.086	2.107
	Rh–I	2.739	2.715	2.758	2.740
	Rh–C	2.123	2.112	2.112	2.121
	O–Rh–O′	91.9	92.5	91.7	91.7
	O′–Rh–C	87.3	86.8	86.6	86.7
	C–Rh–I	91.7	92.2	92.1	92.2
	I–Rh–O	89.1	88.6	89.6	89.5
	P–Rh–P′	173.0	173.8	179.7	176.4
	RMSD	–	0.02	0.10	0.13
	ΔE_{TBE}	21	16	−29	−23
Alkyl-C	Rh–P	2.511	2.457	2.416	2.460
	Rh–P′	2.257	2.229	2.227	2.260
	Rh–O	2.121	2.102	2.134	2.133
	Rh–O′	2.090	2.073	2.104	2.095
	Rh–I	2.757	2.732	2.742	2.761
	Rh–C	2.114	2.106	2.131	2.120
	O–Rh–O′	91.5	92.0	91.8	91.3
	O′–Rh–P′	90.5	90.2	85.2	89.6
	P′–Rh–I	89.3	89.7	93.9	93.5
	I–Rh–O	88.0	87.5	88.9	85.1
	P–Rh–C	167.6	167.6	175.6	172.2
	RMSD	–	0.03	0.16	0.16
	ΔE_{TBE}	12	2	−33	−48
Alkyal-D	Rh–P	2.294	2.267	2.277	2.251
	Rh–P′	2.261	2.232	2.264	2.236
	Rh–O	2.121	2.102	2.134	2.163
	Rh–O′	2.179	2.159	2.210	2.205
	Rh–I	2.821	2.795	2.847	2.853
	Rh–C	2.126	2.112	2.112	2.115
	O–Rh–O′	90.1	90.6	88.9	89.2
	O′–Rh–P′	93.1	92.5	96.0	85.9
	P′–Rh–C	87.7	88.5	88.4	94.5
	C–Rh–O	88.9	88.1	86.6	90.4
	P–Rh–I	166.6	166.9	174.6	175.1
	RMSD	–	0.02	0.12	0.12
	ΔE_{TBE}	−3	−14	−56	−77

of the corresponding angle for the three models. It is expected that the bond angles around the Rh center will differ as the size of the R group increases from H to CH_3 to Ph. The C_{CH_3}–Rh–I angle of the full experimental model of Alkyl-A is 169.1° and is in the same order as the C_{CH_3}–Rh–I angle (174.2°) of *trans*-[Rh(*N*-benzoyl-*N*-phenylhydroxyamino)(P(OPh)$_3$)$_2$(CH$_3$)(I)] and the I–Rh–I angle (*ca.* 170°) in the similar complex [Rh(tfaa)(P(OPh)$_3$)$_2$(I)$_2$] [31]. The slightly distorted octahedral arrangement in [Rh(tfaa)(P(OPh)$_3$)$_2$(I)$_2$] is attributed to the steric interaction between the iodide and triphenylphosphite ligands. The calculated C_{CH_3}–Rh–I angle of the simplified models of Alkyl-A, however, increases with decreasing P(OR)$_3$ groups – 171.7° and 176.5° for [Rh(acac)(P(OCH$_3$)$_3$)$_2$(CH$_3$)(I)] and [Rh(acac)(P(OH)$_3$)$_2$(CH$_3$)(I)] respectively.

The deviation of the geometry of the two simplified models can also be evaluated by comparing the RMSD values of the key bonds of the Rh(CCOCCOC)(P)$_2$ backbone of the optimized simplified model, fitted on the backbone of the optimized full model (Table 2). The RMSD values of the simplified rhodium(I) models are exceptionally good (0.06 and 0.09 Å respectively). The RMSD values of the simplified rhodium(III) models (between 0.10 and 0.16 Å) are somewhat larger than the rhodium(I) values, as would be expected for the more complex molecules. Therefore, both simplified models (R = CH$_3$ or H) give a good account of the key bond lengths around the rhodium center relative to that of the full experimental model.

3.4. Transition state of acetylacetonatobis(triphenylphosphite) rhodium and simplified models

Fig. 4 displays the three types of TS structures that have been reported for the oxidative addition of methyl iodide to square planar rhodium(I) complexes (especially the Monsanto catalyst [Rh(CO)$_2$I$_2$]$^-$) [37,3]. Two results from *trans* addition ("linear" and "bent") and one results from *cis* addition ("front"). The linear TS structure corresponds to a S_N2 mechanism, characterized by a linear Rh–C_{CH_3}–I arrangement and by a Rh–C_{CH_3}–H angle close to 90°. The methyl hydrogen atoms are located in the equatorial plane of the five-coordinated carbon atom, resulting in a trigonal bipyramidal arrangement. The bent and front TS structures correspond to a side-on approach of the C_{CH_3}–I bond to the rhodium atom. The bent transition state structure leads to the same intermediate product as the linear transition state structure – a cationic five-coordinated rhodium complex and a free iodide ion [3]. Both the mechanisms of the linear and the bent transition state structures are therefore described as S_N2 processes. The front TS structure corresponds to a concerted three-center oxidative addition, in which the Rh–I and Rh–C_{CH_3} bonds form simultaneously as the I–C_{CH_3} bond breaks, resulting in the *cis* addition of the methyl iodide. Table 3 summarizes the main geometric parameters of the TS structures determined for the simplified models in the present study, as well as calculated geometric parameters of the Monsanto catalyst [Rh(CO)$_2$I$_2$]$^-$ [37].

The three types of TS structures exhibit similar characteristics. The I–C_{CH_3} bond length and the Rh–C_{CH_3} bond distances for all the

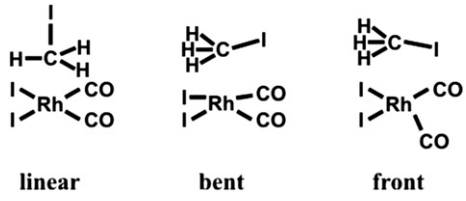

Fig. 4. Schematic illustration of a linear, bent and front transition state for the nucleophilic attack of square planar rhodium(I) on methyl iodide. The Monsanto catalyst [Rh(CO)$_2$I$_2$]$^-$ is used in this figure as example for the square planar rhodium(I) complex.

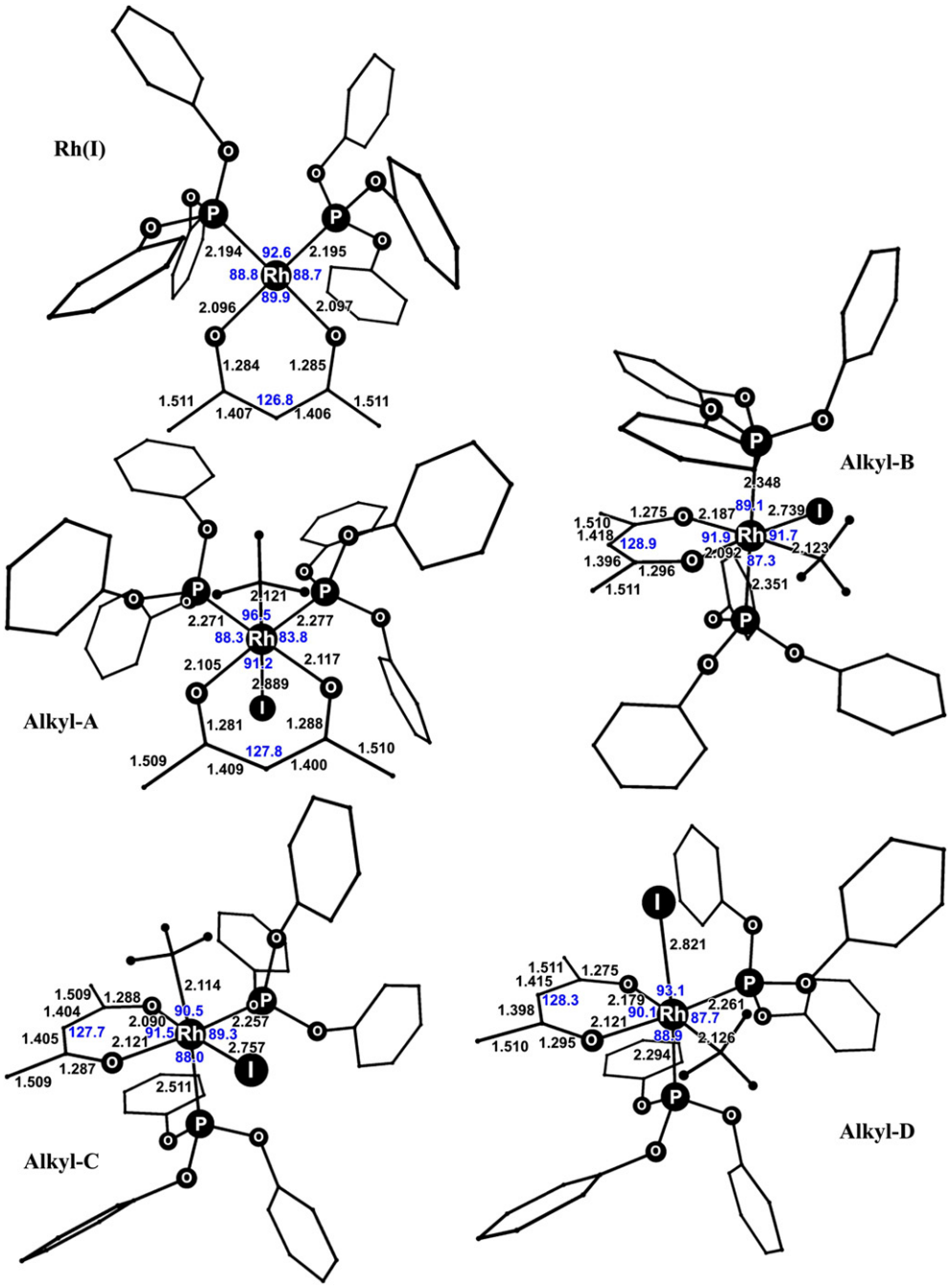

Fig. 5. The PW91/TZP/methanol calculated minimum energy geometries of the [Rh(acac)(P(OPh)$_3$)$_2$] complex and the four possible [Rh(acac)(P(OPh)$_3$)$_2$(CH$_3$)(I)]-alkyl reaction products. The H atoms are removed for clarity (except for the CH$_3$ group bonded to the rhodium). Bond angles (°) and bond lengths (Å) are as indicated. (Only angles in the square planar plane are given).

[Rh(acac)(P(OH)$_3$)$_2$(CH$_3$)(I)] and [Rh(acac)(P(OCH$_3$)$_3$)$_2$(CH$_3$)(I)] TS structures, as well as the Monsanto TS structures, are very similar (2.51–2.85 Å and 2.54–2.78 Å respectively). The Rh–C$_{CH_3}$–I angles are between 172.9 and 176.7° for the linear TS structures, 89.2–95.0° for the bent TS structures and 64.3–68.1° for the front TS structures. The linear transition state, as was also found for the Monsanto catalyst [37], is favored by a large margin of energy (>90 kJ mol^{-1}) with activation barriers ($\Delta E^{\neq}_{TBE}$) of 14–32 kJ mol^{-1}. The bent and front transition states were therefore not considered in further investigations. The calculated relative energies for the reactants, linear TS structures and products are summarized in Fig. 3. The thermochemical data are summarized in Table 4. The calculated enthalpy of activation ($\Delta H^{\neq}$) is between 19 and 37 kJ mol^{-1} for the different models. The large negative entropy of activation ($\Delta S^{\neq}$) calculated for all models, is consistent with an associative mechanism. The activation free energy ($\Delta G^{\neq}$) of the two simplified models (60 kJ mol^{-1} for both models) is lower than that of the full model (75 and 78 kJ mol^{-1}, with and without relativistic effects).

The DFT optimized reactant complexes, the linear TS and the reaction intermediate for the [Rh(acac)(P(OPh)$_3$)$_2$] + CH$_3$I reaction are visualized in Fig. 6. The metal center attacks the methyl group in a S$_N$2-type fashion, approaching the methyl iodide *trans* to the leaving iodide group. During this process the metal–methyl bond is under development, whereas the methyl–iodide bond is

Table 3
The PW91/TZP/methanol calculated selected geometrical parameters, TS imaginary frequencies and activation energies ($\Delta E^{\neq}_{TBE}$) of three possible transitions states when methyl iodide is oxidatively added to the selected square planar rhodium(I) complexes.

	Freq/cm^{-1}	Intensity	$d_{Rh-C(CH3)}$/Å	$d_{C(CH3)-I}$/Å	$a_{Rh-C(CH3)-I}$/°	a_{I-C-H}/°	$\Delta E^{\neq}_{TBE}$/kJ mol^{-1}
[Rh(acac)(P(OH)$_3$)$_2$(CH$_3$)(I)]							
Linear	−242	−523	2.541	2.554	172.9	93.2	14
Bent	−523	−315	2.678	2.845	95.0	78.8, 149.6	155
Front	−253	−43	2.689	2.617	65.1	83.0, 112.0	106
[Rh(acac)(P(OCH$_3$)$_3$)$_2$(CH$_3$)(I)]							
Linear	−187	−514	2.608	2.509	175.4	95.5	17
Bent	−311	−305	2.684	2.862	94.0	70.4, 136.7	14
Front	−264	−82	2.655	2.522	68.1	86.9, 119.9	161
[Rh(CO)$_2$I$_2$(CH$_3$)(I)]$^{-}$[a]							
Linear	−323	–	2.592	2.577	176.7	91.8	32
Bent	−386	–	2.775	2.641	89.2	144.2, 81.9	160
Front	−306	–	2.618	2.721	64.3	124.5, 95.5	157

[a] From Ref. [37].

substantially stretched. In the reactant [Rh(acac)(P(OPh)$_3$)$_2$], the large OPh groups are bent backwards so that the Ph groups are arranged above, below and in the square planar plane (formed by the acac-ligand, the rhodium atom and the two phosphor atoms). As the CH$_3$I group approaches the reactant, the "arms" of the OPh groups above the plane gradually open up to accept the incoming CH$_3$I group to proceed through the TS. The overall structure of the TS appears to be square pyramidal, with the CH_3^+ group in the pyramidal position (Fig. 6, *Middle*). The optimized distance between the attacking rhodium atom and CH_3^+ group at the point of the TS is 2.55, 2.61 and 2.54 Å respectively for R = Ph, CH$_3$ and H. The carbon–iodide bond distance of the CH$_3$I group increased from 2.18 Å in the reactant to 2.59, 2.51 and 2.55 Å in the transition state (R = Ph, CH$_3$ and H).

Rhodium(I) is a $d^2_{xz}d^2_{xz}d^2_{xy}d^2_{z2}d^0_{x2-y2}$ complex of which the HOMO (highest occupied molecular orbital) exhibits mainly $d_{z^2}^2$ character. The HOMO of the TS is visualized in Fig. 6 (*Middle*). The main contribution to the Rh–C_{CH_3} bond in the TS comes from the overlap of the d_{z2} HOMO of the rhodium atom with the p_z LUMO (lowest unoccupied molecular orbital) of the methyl carbon.

Following the TS, is the formation of the cationic five-coordinate [Rh(acac)(P(OPh)$_3$)$_2$(CH$_3$)]$^+$ intermediate with the CH$_3$ group in the apical position (Fig. 6, *right*) and with the iodide ion drifting away into the solvent sphere. The product, [Rh(acac)(P(OPh)$_3$)$_2$(CH$_3$)(I)] Alkyl-A, is octahedral with the methyl and iodide above and below the square planar plane in a *trans* arrangement (Fig. 5, Alkyl-A). Inversion of configuration at the methyl carbon occurred and the methyl group is fully bonded to rhodium atom.

3.5. Calculated vs. experimental thermochemical data

The obtained thermochemical data (Table 4) can be compared to experimental [8] results. The activation enthalpy ($\Delta H^{\neq}$) for the oxidative addition of CH$_3$I to [Rh(acac)(P(OPh)$_3$)$_2$] is experimentally determined as 40(3) kJ mol^{-1}, which is in the same order as the calculated activation enthalpy value of 37 and 28 kJ mol^{-1} determined without and with relativistic effects respectively. The calculated values for the two simplified models are lower, 22 and 19 kJ mol^{-1} for [Rh(acac)(P(OCH$_3$)$_3$)$_2$] and [Rh(acac)(P(OH)$_3$)$_2$] respectively. The entropy of activation ($\Delta S^{\neq}$) of the reaction [Rh(acac)(P(OPh)$_3$)$_2$] + CH$_3$I is experimentally determined as −128(9) kJ mol^{-1}. This is in agreement with the large negative activation entropy observed for all models here. The activation free energy ($\Delta G^{\neq}$) of the reaction [Rh(acac)(P(OPh)$_3$)$_2$] + CH$_3$I is experimentally determined as 78 kJ mol^{-1}, which is in high agreement with the calculated values of 75 and 78 kJ mol^{-1} for the full model (determined without and with relativistic effects). The calculated values of the two simplified models failed to accurately reproduce this value (60 kJ mol^{-1} for both [Rh(acac)(P(OCH$_3$)$_3$)$_2$] and [Rh(acac)(P(OH)$_3$)$_2$]). The agreement between experiment and theory for the individual components $\Delta H^{\neq}$ and $\Delta S^{\neq}$ to $\Delta G^{\neq} = H^{\neq} - T\Delta S^{\neq}$ is thus not as good as for $\Delta G^{\neq}$ itself. The large compensating variations $\Delta H^{\neq}$ and $\Delta S^{\neq}$ with a modest change in $\Delta G^{\neq}$ were also found by Ziegler and assigned to solvent effects [7].

A reduction in the activation enthalpy associated with the oxidative addition reaction [Rh(acac)(P(OR)$_3$)$_2$] + CH$_3$I is observed for R = CH$_3$ as compared to Ph. On the basis of Tolman's electronic parameter (Table 5), P(OCH$_3$)$_3$ is expected to be somewhat more electron-rich than P(OPh)$_3$ [38]. Therefore, nucleophilic attack of the rhodium atom of [Rh(acac)(P(OCH$_3$)$_3$)$_2$] on the CH_3^+ group is expected to be easier than that of [Rh(acac)(P(OPh)$_3$)$_2$]. The higher calculated activation enthalpy of [Rh(acac)(P(OPh)$_3$)$_2$] + CH$_3$I is therefore as expected on electronic grounds. However, the bulkiness of the P(OPh)$_3$ group could hinder the attack of the rhodium atom of [Rh(acac)(P(OPh)$_3$)$_2$] on the CH_3^+ group, also leading to a higher energy barrier. The high agreement between the computed activation enthalpy for the full experimental model and the experimentally obtained value demonstrates that the use of the full P(OPh)$_3$)$_2$ groups are vital for obtaining accurate theoretical values.

Table 4
The PW91/TZP/methanol calculated thermodynamic data of the reactants, TS and product during the oxidative addition reaction [Rh(acac)(P(OR)$_3$)$_2$] + CH$_3$I (where R = Ph, CH$_3$ or H). All energy values are given compared to the reactant. Unbracket values refer to R = Ph, round bracket values refer to R = Ph (including relativistic effects), square bracket values refer to R = CH$_3$ and curved bracket values refer to R = H. Experimental activation parameters are in italics.

	ΔE_{TBE}/kJ mol^{-1}[a]	$\Delta H^{298\ K}$/kJ mol^{-1}[a]	$\Delta G^{298\ K}$/kJ mol^{-1}[b]	$\Delta S^{298\ K}$/J K^{-1} mol^{-1}[c]
Reactant	0 (0) [0] {0}	0 (0) [0] {0}	0 (0) [0] {0}	0 (0) [0] {0}
TS	30 (22) [14] {17}	37 (28) [22] {19} *40(3)*[d]	75 (78) [60] {60} *78*[d]	−129 (−168) [−125] {−137} – *128(9)*[d]
Product (Alkyl-A)	−28 (−34) [−71] {−101}	−16 (−27) [−56] {-95}	27 (18) [−2] {−47}	−144 (−151) [−180] {−163}

[a] Enthalpy, calculated by Equation (2).
[b] Gibbs free energy, calculated by Equation (3).
[c] Entropy, calculated from the temperature dependent partition function in ADF at 298 K.
[d] Experimental activation parameters from Ref. [8b].

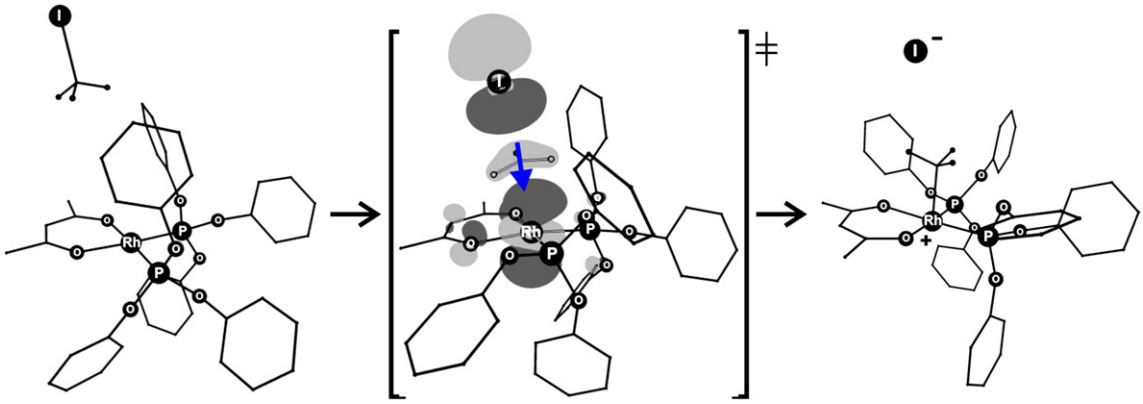

Fig. 6. The PW91/TZP/methanol optimized structures of the oxidative addition of the reaction [Rh(acac)(P(OPh)$_3$)$_2$] + CH$_3$I. The H atoms are removed for clarity (except for the methyl group of the CH$_3$I). *Left*: The reactant complexes *viz.* [Rh(acac)(P(OPh)$_3$)$_2$] + CH$_3$I. *Middle*: The square pyramidal TS, involving the attack of rhodium atom on the CH_3^+ group with displacement vector (blue arrow), indicating movement of the CH_3^+ group at the negative frequency (−258.6 cm^{-1}). The HOMO of the TS is superimposed on the TS geometry – note the d_{z2} orbital on the rhodium center. *Right*: The optimized reaction intermediate [Rh(acac)(P(OPh)$_3$)$_2$(CH$_3$)]$^+$I$^-$ (For interpretation of the references to colour in this figure legend, the reader is referred to the web version of this article).

Table 5
Electronic (ν) and steric (cone angle θ) parameters of P(OR)$_3$, R = Ph or CH$_3$ and computed relative activation enthalpies for oxidative addition reaction [Rh(acac)(P(OR)$_3$)$_2$] + CH$_3$I.

P(OR)$_3$	ν/cm^{-1}	Cone angle/°	$\Delta H^{\neq}$ $^{298\ K}$/kJ mol^{-1}
P(OPh)$_3$	2085.3	128	37
P(OCH$_3$)$_3$	2079.5	107	22

The calculated activation barrier, $\Delta E_{TBE}^{\neq} = 30$ kJ mol^{-1}, for the *trans* addition of CH$_3$I to [Rh(acac)(P(OPh)$_3$)$_2$] in this study is of the same order as the reported DFT values for the Monsanto system 32 kJ mol^{-1} (Table 3, BP86) by Feliz [37], but smaller than the value reported by Laasonen when using the hybrid B3LYP functional (68 kJ mol^{-1}) [5b]. The calculated thermochemical quantities ($\Delta S^{\neq}$, $\Delta H^{\neq}$, $\Delta G^{\neq}$, 298 K) of this study compare well with experimental data of the Monsanto catalyst, −120 J mol^{-1} K^{-1}, 60 kJ mol^{-1} and 96 kJ mol^{-1} respectively [3]. However, since the [Rh(acac)(P(OPh)$_3$)$_2$] complex in this study does not contain a CO group, no methyl migration, the second step in the Monsanto catalytic cycle, is possible. The potential use of [Rh(acac)(P(OPh)$_3$)$_2$] in industry other than olefin hydroformylation [39], thus still has to be further explored.

4. Conclusion

Simplified model systems for the oxidative addition reaction [Rh(acac)(P(OPh)$_3$)$_2$] + CH$_3$I, *viz.* [Rh(acac)(P(OCH$_3$)$_3$)$_2$] and [Rh(acac)(P(OH)$_3$)$_2$], give a good account of the Rh-L experimental bond lengths of both rhodium(I) and rhodium(III) β-diketonatobis(triphenylphosphite) complexes. All models give the same trend concerning the relative stability of the four possible rhodium(III) reaction products. The main features of the TS, *viz.* the nucleophilic attack of the rhodium atom on the CH_3^+ group and the cleavage of the carbon–iodide bond, are similar for all three systems. Therefore, in order to save on computational recourses, a simplified model system can be used to obtain preliminary information of the oxidative addition reaction of CH$_3$I to [Rh(β-diketonato)(P(OPh)$_3$)$_2$] complexes. However, for the best agreement with experimental activation parameters, the full experimental system is necessary.

Acknowledgments

Financial assistance by the South African National Research Foundation (grant number 65507) and the Central Research Fund of the University of the Free State is gratefully acknowledged.

Appendix. Supporting information

Additional figures and tables (as described in the text) and Cartesian coordinates (in Å) of the structures associated with this study.

The supplementary data associated with this article can be found in the on-line version at doi:10.1016/j.jorganchem.2010.05.021.

References

[1] (a) P.M. Maitlis, A. Haynes, G.J. Sunley, M.J. Howard, J. Chem. Soc. Dalton Trans. (1996) 2187–2196;
(b) L. Cavallo, M. Sola, J. Am. Chem. Soc. 123 (2001) 12294–12302;
(c) A. Haynes, P.M. Maitlis, G.E. Morris, G.J. Sunley, H. Adams, P.W. Badger, C.M. Bowers, D.B. Cook, P.I.P. Elliott, T. Ghaffer, H. Green, T.R. Griffin, M. Payne, J.M. Pearson, M.J. Taylor, P.W. Vickers, R.J. Watt, J. Am. Chem. Soc. 126 (2004) 2847–2861.
[2] (a) L. Gonsalvi, H. Adams, G.J. Sunley, F. Ditzel, A. Haynes, J. Am. Chem. Soc. 121 (1999) 11233–11234;
(b) L. Gonsalvi, H. Adams, G.J. Sunley, F. Ditzel, A. Haynes, J. Am. Chem. Soc. 124 (2002) 13597–13612;
(c) J. Rankin, A.C. Benyei, A.D. Poole, D.J. Cole-Hamilton, J. Chem. Soc. Dalton Trans. (1999) 3771–3782;
(d) D. Forster, J. Am. Chem. Soc. 98 (1976) 846–848;
(e) D. Forster, Adv. Organomet. Chem. 17 (1979) 255–267;
(f) A. Haynes, B.E. Mann, G.E. Morris, P.M. Maitlis, J. Am. Chem. Soc. 115 (1993) 4093–4100;
(g) S.B. Dake, R.V. Chaudhari, J. Mol. Catal. 26 (1984) 135–138.
[3] T.R. Griffin, D.B. Cook, A. Haynes, J.M. Pearson, D. Monti, G.E. Morris, J. Am. Chem. Soc. 118 (1996) 3029–3030.
[4] M. Cheong, R. Schmid, T. Ziegler, Organometallics 19 (2000) 1973–1982.
[5] (a) T. Kinnunen, K. Laasonen, J. Mol. Struct. (Theochem) 540 (2001) 91–100;
(b) T. Kinnunen, K. Laasonen, J. Mol. Struct. (Theochem) 542 (2001) 273–288.
[6] E.A. Ivanova, P. Gisdakis, V.A. Nasluzov, A.I. Rubailo, N. Rösch, Organometallics 20 (2001) 1161–1174.
[7] M. Cheong, T. Ziegler, Organometallics 24 (2005) 3053–3058.
[8] (a) J.G. Leipoldt, E.C. Steynberg, R. van Eldik, Inorg. Chem. 26 (1987) 3068–3070;
(b) G.J. van Zyl, G.J. Lamprecht, J.G. Leipoldt, T.W. Swaddle, Inorg. Chim. Acta 143 (1988) 223–227;
(c) G.J. van Zyl, G.J. Lamprecht, J.G. Leipoldt, Inorg. Chim. Acta 129 (1987) 35–37.
[9] V. Chauby, J.-C. Daran, C.S.-L. Berre, F. Malbosc, P. Kalck, O.D. Gonzalez, C.E. Haslam, A. Haynes, Inorg. Chem. 41 (2002) 3280–3290.
[10] (a) J.A. Venter, J.G. Leipoldt, R. van Eldik, Inorg. Chem. 30 (1991) 2207–2209;
(b) M.R. Galding, T.G. Cherkasova, L.V. Osetrova, Y.S. Varshavsky, A. Roodt, Rhodium Express 16 (1996) 23–36;
(c) A. Roodt, J.M. Botha, S. Otto, E.P. Shestakova, Y.S. Varshavsky, Rhodium Express 17 (1996) 4–9.
[11] F.A. Cotton, G. Wilkinson, Basic Inorganic Chemistry. John Wiley & Sons, New York, 1976, pp. 529–547.
[12] Cambridge Structural Database (CSD), Version 5.30, August 2008 update.
[13] G. Te Velde, F.M. Bickelhaupt, E.J. Baerends, C.F. Guerra, S.J.A. Van Gisbergen, J.G. Snijders, T. Ziegler, J. Comput. Chem. 22 (2001) 931–967.

[14] J.P. Perdew, J.A. Chevary, S.H. Vosko, K.A. Jackson, M.R. Pederson, D.J. Singh, C. Fiolhais, Phys. Rev. B 46 (1992) 6671–6687;
Erratum: J.P. Perdew, J.A. Chevary, S.H. Vosko, K.A. Jackson, M.R. Pederson, D.J. Singh, C. Fiolhais, Phys. Rev. B 48 (1993) 4978.
[15] L. Fan, T. Ziegler, J. Chem. Phys. 96 (1992) 9005–9012.
[16] L. Fan, T. Ziegler, J. Am. Chem. Soc. 114 (1992) 10890–10897.
[17] A. Klamt, G. Schüürmann, J. Chem. Soc. Perkin Trans. 2 (1993) 799–805.
[18] A. Klamt, J. Phys. Chem. 99 (1995) 2224–2235.
[19] A. Klamt, V. Jones, J. Chem. Phys. 105 (1996) 9972–9981.
[20] C.C. Pye, T. Ziegler, Theor. Chem. Acc. 101 (1999) 396–408.
[21] J.L. Pascual-Ahuir, E. Silla, I. Tuñon, J. Comput. Chem. 15 (1994) 1127–1138.
[22] E. van Lenthe, A.E. Ehlers, E.J. Baerends, J. Chem. Phys. 110 (1999) 8943–8953.
[23] E. van Lenthe, E.J. Baerends, J.G. Snijders, J. Chem. Phys. 99 (1993) 4597–4610.
[24] E. van Lenthe, E.J. Baerends, J.G. Snijders, J. Chem. Phys. 101 (1994) 9783–9792.
[25] E. van Lenthe, J.G. Snijders, E.J. Baerends, J. Chem. Phys. 105 (1996) 6505–6516.
[26] E. van Lenthe, R. van Leeuwen, E.J. Baerends, J.G. Snijders, Int. J. Quantum Chem. 57 (1996) 281–293.
[27] G.A. Zhurko, D.A. Zhurko, Chemcraft, Version 1.6 (Build 304) (2009).
[28] J.G. Leipoldt, G.J. Lamprecht, G.J. Van Zyl, Inorg. Chim. Acta 96 (1985) L31–L34.
[29] G.J. Lamprecht, J.G. Leipoldt, G.J. Van Zyl, Inorg. Chim. Acta 97 (1985) 31–35.
[30] G.J. Van Zyl, G.J. Lamprecht, J.G. Leipoldt, Inorg. Chim. Acta 102 (1985) L1–L4.
[31] G.J. Van Zyl, G.J. Lamprecht, J.G. Leipoldt, Inorg. Chim. Acta 122 (1986) 75–79.
[32] (a) A.C. Scheiner, J. Baker, J.W. Andzelm, J. Comput. Chem. 18 (1997) 775–795;
(b) J.R. Hill, C.M. Freeman, B. Delley, J. Phys. Chem. A 103 (1999) 3772–3777;
(c) F. Furche, J.P. Perdew, 124 (2006) 044103.
[33] W.J. Hehre, A Guide to Molecular Mechanics and Quantum Chemical Calculations, vol. 181, Wavefunction Inc., 2003, p. 153.
[34] When optimizing the full experimental model, the influence of the rotating OPh groups must be taken into account so that the geometry of the global minimum energy structures (in solution) of [Rh(acac)(P(OPh)$_3$)$_2$] (1) and the four possible alkyl [Rh(acac)(P(OPh)$_3$)$_2$(CH$_3$)(I)] products can be obtained. A conformational search was thus performed by calculating the energy of the molecules as a function of the (Oacac)-Rh-P-O dihedral angle. The global minimum energy structure was then obtained by re-optimizing the minimum energy structure obtained from the dihedrally restricted optimizations, without any restraints.
[35] G.J. Lamprecht, G.J. Van Zyl, J.G. Leipoldt, Inorg. Chim. Acta 164 (1989) 69–72.
[36] (a) M.M. Conradie, J. Conradie, Inorg. Chim. Acta 362 (2009) 519–530;
(b) M.S. Stuurman, J. Conradie, J. Organomet. Chem. 694 (2009) 259–268;
(c) M.M. Conradie, J. Conradie, Inorg. Chim. Acta 361 (2008) 208–218;
(d) M.M. Conradie, J. Conradie, S. Afr. J. Chem. 61 (2008) 102–111;
(e) M.M. Conradie, J. Conradie, Inorg. Chim. Acta 361 (2008) 2285–2295.
[37] M. Feliz, Z. Freixa, P.W.N.M. van Leeuwen, C. Bo, Organometallics 24 (2005) 5718–5723.
[38] C.A. Tolman, Chem. Rev. 77 (1977) 313–384.
[39] (a) A.M. Trzeciak, J. Organomet. Chem. 390 (1990) 105–111;
(b) A.M. Trzeciak, T. Głowiak, R. Grzybek, J.J. Ziolkowski, J. Chem. Soc. Dalton Trans. (1997) 1831–1837;
(c) A.M. Trzeciak, E. Mieczynska, J.J. Ziolkowski, Top. Catal. 11 (2000) 461–468.